Vertically aligned CdTe nanotube arrays on indium tin oxide for visible-light-driven photoelectrocatalysis

Xina Wang [a,b], Guisheng Li [c,d], Haojun Zhu [a], Jimmy C. Yu [c], Xudong Xiao [a], Quan Li [a,*]

[a] Department of Physics, The Chinese University of Hong Kong, Shatin, New Territory, Hong Kong, China
[b] Faculty of Physics and Electronic Technology, Hubei University, Wuhan 430062, China
[c] Department of Chemistry, The Chinese University of Hong Kong, Shatin, New Territory, Hong Kong, China
[d] College of Life and Environmental Science, Shanghai Normal University, Shanghai 200234, China

ARTICLE INFO

ABSTRACT

Vertically aligned CdTe nanotube arrays with visible-light-driven photoelectrocatalytic (PEC) activity were grown on ITO substrate via a simple ZnO nanorod-templating method. The high crystallinity, strong absorption of visible-light, and vertical arrays architecture were found to be beneficial for the photoelectrodegradation of Acid Blue 80. Together with the detailed microstructure and photoelectric response over visible light, a photoelectrocatalysis mechanism based on the energy diagram was proposed for the CdTe nanotube arrays. Further enhancement in the PEC property can be expected when the configuration was optimized, such as sample size, nanotube length and coupling with other metal/semiconductor on ITO. This study provides a good strategy for the design of visible light-responsive photocatalysts that can be recycled and possess high efficiency, extremely low mass and high chemical stability together.

© 2013 Elsevier B.V. All rights reserved.

1. Introduction

To better utilize solar energy and develop environmental cleaning by decomposing organic contaminants, intensive research efforts have been devoted to the development of semiconductor-based photocatalysts. A good photocatalyst should have strong visible light absorption and fast charge separation [1]. To this point, nanomaterial is generally preferred for their large surface area suitable for catalytical applications [2]. Among the various semiconductor photocatalysts, TiO_2 has been the most successful one because of its high photostability, low cost and non-toxicity [3–7]. Though functionalizations of TiO_2 were adopted through coupling with other semiconductor systems (e.g. TiO_2–SnO_2, TiO_2–WO_3, TiO_2–CdS coupled photocatalysts) [8–15], or anion-doping such as N, C and F, etc. [16–18], the absorption is mainly located within the UV range. A number of semiconductors with narrower bandgap such as WO_3, Fe_2O_3, CdS, CdSe, InP and PbS have been attempted [19–24], but the catalytic performance upon visible light remains a big challenge. In most cases, the photocatalysts were adopted as powders suspended in water, which limit their practical application because of the laborious recollection and recycling difficulty of the powders from a suspension.

On the other hand, applying a small bias on photocatalytic nanoparticle film is believed to be an efficient way to enhance the photodegradation efficiency by decreasing carrier recombinations and promoting charge separation [25,8,26,27]. For most photocatalysis, the major oxidizing species is attributed to OH radicals formed via oxidation of hydroxide ions by photoexcited holes in the valence band of the catalyst [28–31]. A rate-determining step in the decolorization process is the simultaneous reduction or scavenge of the trapped photogenerated electrons at the valence band of catalyst. Failure to scavenge electrons with a sacrificial electron-acceptor results in high carrier recombination and low photocatalytic efficiency. Unlike in slurry system, applying an anodic bias on catalyst electrode can help to drive away the trapped electrons from the conduction band of the catalyst to the external circuit in the absence of electron scavengers, while the left holes were scavenged by H_2O molecules adsorbed on the catalyst surface [8]. In this regard, 1D array is preferred for it provides direct channels for carrier transport so as to reduce carrier scattering and recombination at surface/boundaries of conventional nanoparticle films [32–34]. Indeed, some demonstrations available are mainly on TiO_2 nanotube arrays [35–37], but not on many other semiconductor systems due to the difficulty in the growth directly on electric conducting substrate and in an array morphology. Compared with the widely reported hybrid catalysts, such as TiO_2–SnO_2, TiO_2–WO_3 and TiO_2–CdS, CdTe related materials grown on ITO substrates may serve as efficient visible light-driven photocatalysts due to its band

---

* Corresponding author. Tel.: +852 3943 6323.
E-mail address: liquan@phy.cuhk.edu.hk (Q. Li).

edge of 1.5 eV and effective charge separation owing to its band structure [38].

In the present work, CdTe NT arrays-on ITO, which enjoy even larger surface compared to nanowires, were demonstrated as effective photoelectrocatalysts to visible light of Acid Blue 80. Together with the microstructure and adsorption property as revealed, a detailed photocatalytic mechanism with the assistance of applied voltage was given. As the nanotube arrays samples were synthesized using electrodepositing method, which is cheap and can be scaled up, it can be applied to a variety of semiconducting materials and for various applications.

2. Experimental

2.1. Sample synthesis

The CdTe nanotube arrays samples have been synthesized via a two-step method using ZnO nanorod array-on-ITO as the template. Firstly, CdTe is grown onto the ZnO nanorods surface in the arrays using electrodeposition, which is carried out in a neutral pH electrolyte using an electrochemical workstation (CH Instrument, model 600B). The ZnO nanorod arrays-on-ITO, Pt foil and a standard saturated calomel electrode (SCE) are used as the working electrode, the counter electrode and the reference electrode, respectively. The electrodeposition is performed at a fixed potential of -1.0 V vs SCE for 30 min in an aqueous electrolyte composed of 0.005 M potassium tellurite (K_2TeO_3), 0.05 M nitrilotriacetic acid trisodium salt (NTA), and 0.02 M cadmium acetate with pH 8.0–8.5. The total charge quantity during the electrodeposition process is 1.4 Q. A core–shell ZnO–CdTe nanocable array is then expected on the ITO substrate as the result of the first step. Secondly, the ZnO–CdTe nanocable arrays sample is dipped into a 25% ammonia aqueous solution for 80 min to completely etch off the ZnO nanorod-cores, leaving CdTe nanotube arrays standing on the ITO substrate. Finally, both the CdTe nanotube arrays and ZnO–CdTe nanocable arrays are annealed at 350 °C for 1 h in Ar atmosphere.

2.2. Structural, optical and photoresponse characterization

The morphology, chemical composition and microstructure of the samples have been characterized using field-emission scanning electron microscopy (FE-SEM, FEI Quantum F400) and scanning transmission electron microscopy (STEM, TEM, Tecnai 20, FEG, equipped with an energy dispersive X-ray (EDX) spectrometer), and X-ray diffraction (XRD, Ragiku RU300). The optical absorption measurements have been performed using a UV-VIS-IR spectrometer (U3501) at room temperature.

2.3. Photoelectrochemical property measurement

Photoelectrochemical measurements have been performed on an electrochemical workstation (CHI660C) in a typical three-electrode system. CdTe nanotube arrays on ITO, Pt foil and SCE were employed as the working electrode, the counter electrode and the reference electrode, respectively. 1 M Na_2SO_4 aqueous solution has been employed as the electrolyte. Photocurrent–voltage curve were measured under AM1.5G light with a power density of 100 mW/cm^2.

2.4. Photoelectrocatalytic degradation measurement

The PEC decolorization of Acid Blue 80 was performed in a single photoelectrochemical reactor constructed of a 100 ml quartz beaker, a CdTe nanotube arrays-on-ITO substrate catalyst serving as photo-anode while a Pt foil as cathode. Before each test, vigorous stirring of the Acid Blue 80 solution (with a concentration of 0.004 g/L and using 0.01 M $(NH_4)_2SO_4$ as the electrolyte) was performed for 30 min in the dark to establish an adsorption–desorption equilibrium among the CdTe nanotube arrays catalyst, dye molecules and water. Three 8 W-UVA lamps and a 100 W-tungsten were used as respective UV and visible light source, both of which were placed 8 cm away from the photo-anode. A constant bias potential at 1.5 V, which is less than the oxidation potential of Acid Blue 80, was applied on the photo-anode during the irradiation process. After irradiation with a time interval of 20 min, the photoelectrocatalytic performance of the nanotube arrays was immediately gauged by measuring the intensity changes of the optical absorption peaks at 626 nm by an UV-VIS-IR spectrometer (U3501). Analogous control experiments were carried out by using a ZnO–CdTe nanocable arrays-on-ITO sample under the same test condition.

3. Results and discussion

3.1. Morphology and microstructure of CdTe nanotube arrays on ITO

Fig. 1a–c are SEM images illustrating the formation process of CdTe nanotube arrays on ITO. Uniform ZnO nanorod arrays were firstly grown on ITO glass with controllable diameter and length. An example of such nanorod array is shown in Fig. 1a, in which the average diameter and length of the ZnO nanorod in the array are ~200 nm and ~10 μm, respectively. The ZnO surface is found to be covered with a layer of material after the CdTe electrodeposition, and its thickness is estimated as ~105 nm. Deposition rate of CdTe on the ZnO top surface is not uniform and relatively slow as compared to that of the side surface deposition. As a result, partial coverage of the ZnO top surface (with the present deposition condition) is found, and an exposed circular area of ~50 nm in diameter is left at the center of the nanorod (Fig. 1b). EDX taken from such a sample discloses the existence of Cd and Te with an atomic ratio close to 1 in addition to Zn and O (Fig. 1f). The ZnO nanorod cores are found to be selectively removed from the nanocables after ammonia etching, leading to nanotube arrays on the ITO substrate (Fig. 1c). The wall thickness and inner diameter of the nanotubes is estimated as ~105 nm and ~200 nm respectively, from the broken nanotubes (Fig. 1d). The length of the nanotube is basically the same as that of the ZnO nanorod. EDX spectrum taken from such a sample reveals the absence of Zn and O signal, while only Cd and Te signal remain with their atomic ratio unchanged. No significant morphological difference is discovered after the nanotube annealing. The above experimental evidence suggests the formation of CdTe nanotube arrays on ITO.

More detailed microstructural information of the CdTe nanotubes can be obtained using TEM-related techniques. The tubular morphology can be clearly observed in the low-magnification TEM image taken from single CdTe nanotube, and the light/dark contrast observed on the nanotube suggests its porous nature. The wall thickness and inner diameter of the nanotube is estimated as ~105 nm and ~200 nm, respectively, being consistent with the SEM results. The spatial distribution of Cd and Te can be found from the abundance profile of the two elements obtained by STEM-EDX line scan taken across the radial direction of the nanocable. The nanotube is polycrystalline (Fig. 2d, a diffraction pattern) with a zinc-blende structure, which can also be observed in the high resolution image taken from a small area of the nanotube. Such a result is well consistent with the XRD pattern (Fig. 3) taken from the sample, in which the diffraction peaks at 23.72°, 39.38°, 46.47°, and 71.28° can be indexed to the (1 1 1), (2 2 0), (3 1 1) and (4 2 2) planes of zincblende
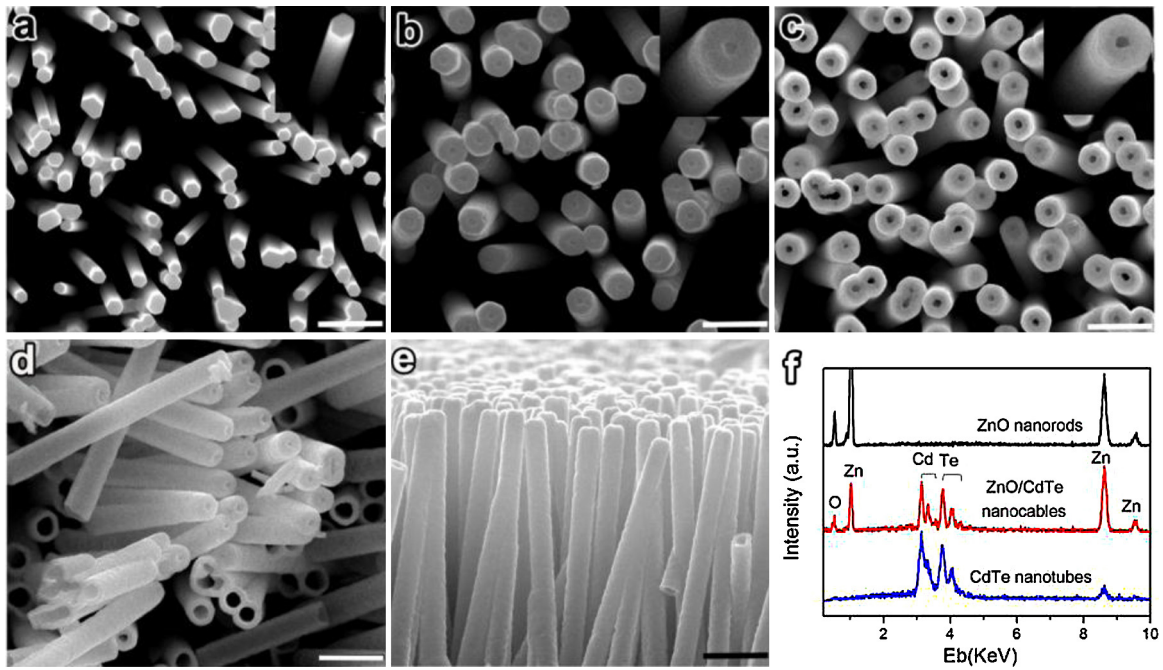
Fig. 1. Top-view SEM images of (a) pure ZnO nanorod arrays, (b) ZnO–CdTe nanocable arrays, (c) and (d) standing and broken CdTe nanotube arrays on ITO detected at different regions of the sample, (e) is a cross-sectional SEM image of CdTe nanotube arrays, and (f) shows the corresponding EDX spectra evolution of the ZnO nanorod arrays, ZnO–CdTe nanocable arrays and CdTe nanotube arrays on ITO substrate. The scale bars are 1 μm.

(ZB) CdTe (JCPDS file No.65-880), respectively. The diffraction peaks denoted by asterisk were derived from ZnO underlayer, which served as the seed layer for ZnO nanorods. This underlayer remains unchangeable after the etching of ZnO nanorods by ammonia.
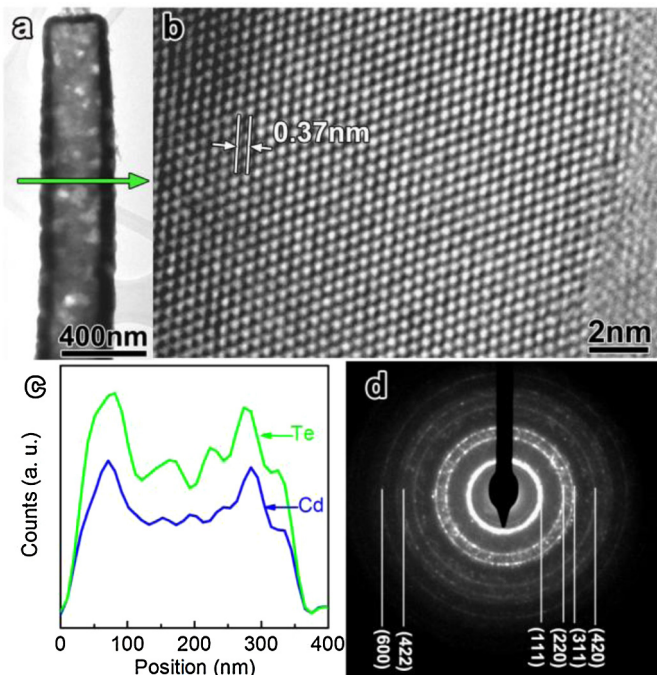

Fig. 2. (a) Low-magnification TEM image showing the uniform morphology of a single CdTe nanotube; (b) elemental profile extract from a STEM-EDX showing the distribution of the compositional elements (Te and Cd) along the radial direction of the nanotube (indicated by the green arrow in (a); (c) HRTEM image taken from the same CdTe nanotube, and (d) A SAED pattern taken from a CdTe nanotube.
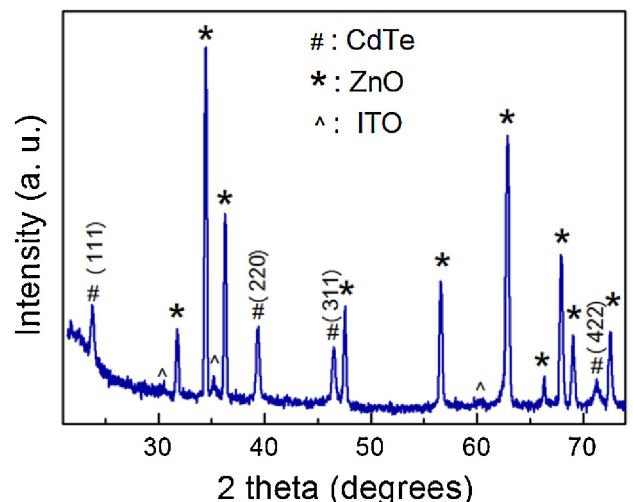
3.2. Absorption and photoresponse of CdTe nanotube arrays

Typical absorption spectra of the ZnO nanorod arrays and the annealed CdTe nanotube arrays on an ITO substrate can be found in Fig. 4. Strong absorption above 3.2 eV can be found in the case of ZnO nanorod array due to its band-edge absorption. As a comparison, an absorption edge redshifts to ~1.5 eV for CdTe nanotube arrays, being consistent with the bandgap of CdTe [38]. This enables the CdTe nanotube arrays to have obvious light absorption in the visible region.

The photoresponse of CdTe nanotube arrays on ITO to visible light was investigated by using a three-electrode photoelectrochemical cell with the nanotube array as the photoanode. Fig. 5 compares the typical current–voltage (I–V) curves obtained in dark and under illumination (AM 1.5G light with a power density of 100 mW/cm^2). No current change is detected when the cell is

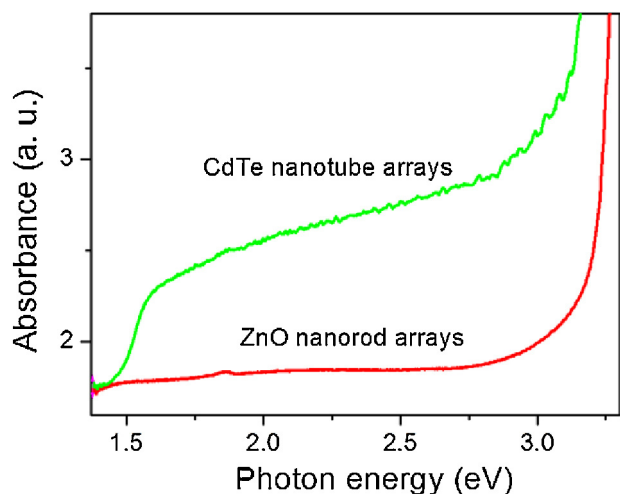**Fig. 3.** XRD pattern of the CdTe nanotube arrays on ITO substrate.

Fig. 4. Absorption spectra of the ZnO nanorod arrays template and post-annealed CdTe nanotube arrays on an ITO substrate.

operated in dark. As a comparison, a surge in current occurs as the potential increased from −0.18 V to 0.37 V (vs SCE). The current increase eventually levels off with further increase in the potential, and reaches a saturation value of ~2.1 mA/cm^2 at ~1.4 V. The remarkable photoresponse of the CdTe nanotube arrays is a direct result of charge carriers generation when excited by incident photons. Short diffusion length associated with the nanotube configuration then facilitates the transport of separated charge carriers to the electrolyte and ITO, respectively, and thus contribute to the photocurrent generation (Fig. 5).

3.3. The photoelectrocatalytic (PEC) activity of CdTe nanotube arrays

The PEC activity of the CdTe nanotube arrays-on-ITO samples was evaluated by photocatalytic decolorization of Acid Blue 80 under UV and visible-light illumination, respectively (Fig. 6). An anodic bias of 1.54 V was applied on the photoelectrode during the irradiation process. It is observed that the photolysis of Acid Blue under both the UV and visible light irradiation is negligible. After 120 min of visible light irradiation, the sample exhibited reduction of 20% of the dye. A reduction of 41% acid blue were achieved when the sample were irradiated by UV light
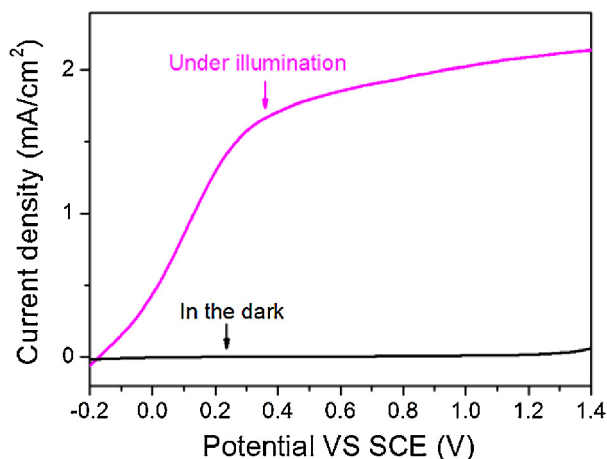

Fig. 5. Current density-potential curves of the CdTe nanotube arrays-on-ITO in 1 M Na$_2$SO$_4$ aqueous solution measured in the dark and under illumination of AM 1.5 light at 100 mW/cm^2 (1 sun).
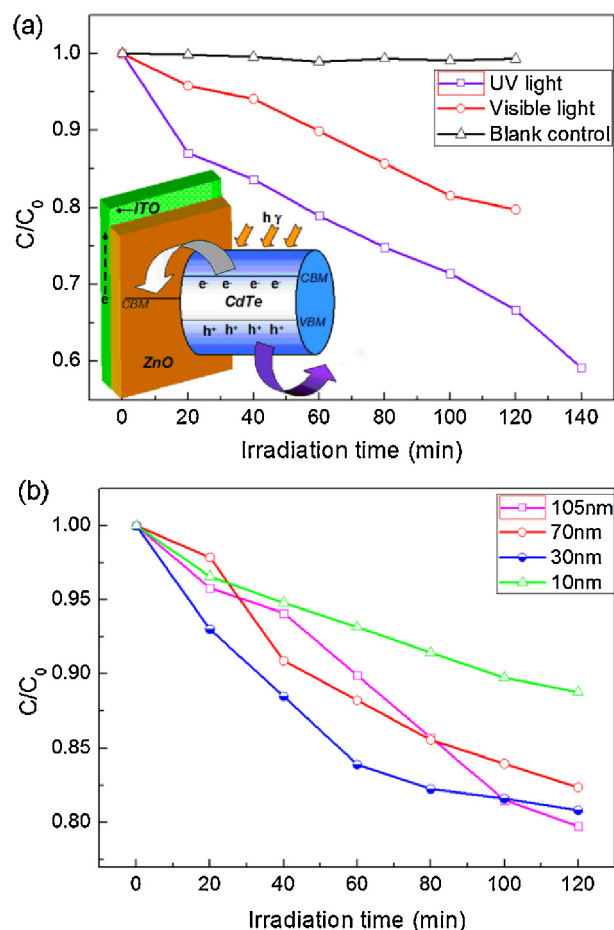

Fig. 6. (a) Photoelectrodegradation of Acid Blue 80 in the presence of a pure CdTe nanotube arrays-on-ITO sample and a ZnO–CdTe nanocable arrays-on-ITO sample. The inset is a schematic diagram of the charge separation in a CdTe nanotube arrays-on-ITO photoanode under applied bias potential. (b) Wall thickness-dependent photodegradation of Acid Blue 80 for the CdTe nanotube arrays when applied an anodic potential of 1.5 V.
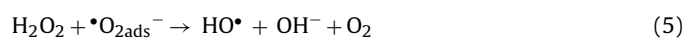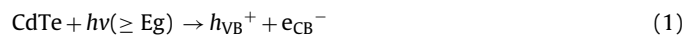
for 140 min. Such a PEC activity is significant when considered the usage amount of CdTe nanotube arrays. According to Faraday's law, 1 F (96487 coulomb) charge across the electrode will have 1 mol electrons transfer in the electrochemical reaction of TeO$_3$$^{2-}$ + 3H$_2$O + Cd^{2+} + 6e → CdTe + 6OH$^-$ [39]. Thus, the photocatalyst used here can be estimated as small as 0.59 mg. Therefore, much higher PEC activity can be expected when the size of the sample was enlarged.

The effect of wall thickness of CdTe nanotube arrays on photocatalysis activity under the visible light was studied. As shown by Fig. 6b, during the former irradiation time of 80 min, the degradation rate increases with the nanotube wall thickness in the order of 30 nm > 70 nm > 105 nm > 10 nm. With the irradiation time extended, the CdTe nanotube arrays with wall thickness of 105 nm showed the best degradation efficiency. At the irradiation time of 120 min, the nanotubes with wall thickness of 30 nm and 70 nm exhibited reduction of 19% and 18%, respectively, a little smaller than that of 105 nm. In comparison, the CdTe nanotubes with wall thickness of 10 nm yield only 11% reduction.

4. Discussion

In order to understand the possible photoelectrocatalytic (PEC) mechanism of CdTe nanotube arrays, parallel experiments were carried out without any bias voltage applied on the above CdTe

nanotube arrays. No significant photodegradation of the dye has been detected. Combined with the energy band offset between CdTe and ITO substrate [40], a scheme related with the photogenerated carrier separation and transfer is illustrated for the CdTe–ITO coupled systems (the inset of Fig. 6a). As reported in our previous work [41], a p–n junction will form at CdTe–ITO interface where both the valance and conduction band of CdTe lie above those of ITO. This makes it energetic reasonable for the photoexcited electrons injecting into ZnO, then being driven away from CdTe via the external circuit, avoiding the need of electron scavengers. When the electrons are transported to Pt electrode, they will react with O_2 and H_2O molecules adsorbed on Pt according to the following pathways (Eqs. (1)–(5)), forming active hydroxyl radicals that can effectively degrade the dye molecules. At the same time, the left photoexcited holes on the valence band of CdTe will participate in the oxidation reaction with the productions formed via the degradation of dyes, combined with the reduction reactions occurring at Pt side, leading to the formation of photocurrent. Note that when a positive potential of 1.5 V is applied on ITO, the barrier height of the p–n junction will increase with the drop of the conduction band of ITO. In this way, the applied positive voltage will make the electrons transfer to ITO become much easier than those without any voltage, greatly decreasing carrier recombinations.

$$CdTe + h\nu(\geq Eg) \rightarrow h_{VB}^+ + e_{CB}^- \qquad (1)$$

$$h_{VB}^+ + e_{CB}^- \rightarrow \text{heat} \qquad (2)$$

$$e_{CB}^- + O_2 \rightarrow {}^\bullet O_2^- \qquad (3)$$

$$2e_{CB}^- + O_2 + 2H^+ \rightarrow H_2O_2 \qquad (4)$$

$$H_2O_2 + {}^\bullet O_{2ads}^- \rightarrow HO^\bullet + OH^- + O_2 \qquad (5)$$

Besides the good CdTe electronic structure quality, the nanotube arrays on ITO configuration also contribute to the photoelectrocatalytic property because it provides a direct channel for the electrons transporting to ZnO layer then to ITO. The nanostructured architecture extending into 3D also results in enhanced effective areas for catalysis as compared with packed free standing structures. In addition, the CdTe nanotube arrays were synthesized by a simple ZnO nanorods-templating method, in which the ZnO nanorods and CdTe were grown via hydrothermal and electrochemical method, respectively, both of which are cheap and scalable. Further enhancement of the PEC property can be expected when the configuration was optimized, such as sample size, nanotube length and coupling with other metal–semiconductor on ITO.

5. Conclusions

In conclusion, high-density CdTe nanotube arrays-on-ITO with various wall thicknesses were synthesized via ZnO nanorod-templating method. The good crystal quality, high absorption over visible light, and the vertical aligned arrays architecture on ITO contribute to the obvious photodegradation property of Acid Blue 80 when applied an anodic bias. Reduction of 20% of the dye was achieved for the CdTe nanotube arrays with a total mass of 0.59 mg, respective length and wall thickness of 10 μm and 105 nm under irradiation of visible light for 120 min. Higher degradation efficiency can be expected due to the advantages including the high surface area of the nanotubes, recyclable, and cheap and scalable character of the method.

References

[1] H. Zhang, G. Chen, D.W. Bahnemann, J. Mater. Chem. 19 (2009) 5089–5121.
[2] D.P. Wang, H.C. Zeng, Chem. Mater. 21 (2009) 4811–4823.
[3] M.R. Hoffmann, S.T. Martin, W. Choi, D.W. Bahnemann, Chem. Rev. 95 (1995) 69–96.
[4] J.G. Yu, S.W. Liu, H.G. Yu, J. Catal. 249 (2007) 59–66.
[5] X.Z. Li, F.B. Li, Environ. Sci. Technol. 35 (2001) 2381–2387.
[6] S.N. Frank, A.J. Bard, J. Am. Chem. Soc. 99 (1977) 303–304.
[7] J.G. Yu, Y.R. Su, B. Cheng, Adv. Funct. Mater. 17 (2007) 1984–1990.
[8] K. Vinodgopal, I. Bedja, P.V. Kamat, Chem. Mater. 8 (1996) 2180–2187.
[9] A. Hattori, Y. Tokihisa, H. Tada, S. Ito, J. Electrochem. Soc. 147 (2000) 2279–2283.
[10] M. Miyauchi, A.K. Nakajima, T. Watanabe, K. Hashimoto, Chem. Mater. 14 (2002) 4714–4720.
[11] S. Higashimoto, M. Sakiyama, M. Azuma, Thin Solid Films 503 (2006) 201–206.
[12] M. Miyauchi, A. Nakajima, K. Hashimoto, T. Watanabe, Adv. Mater. 12 (2000) 1923–1927.
[13] L. Spanhel, H. Weller, A. Henglein, J. Am. Chem. Soc. 109 (1987) 6632–6635.
[14] J.C. Yu, L. Wu, J. Lin, P. Li, Q. Li, Chem. Commun. 9 (2003) 1552–1553.
[15] J.Y. Wang, Z.H. Liu, Q. Zheng, Z.K. He, R.X. Cai, Nanotechnology 17 (2006) 4561–4566.
[16] R. Asahi, T. Morikawa, T. Ohwaki, K. Aoki, Y. Taga, Science 293 (2001) 269–271.
[17] H. Irie, Y. Wanatabe, K. Hashimoto, J. Phys. Chem. B 107 (2003) 5483–5486.
[18] J.C. Yu, J.G. Yu, W.K. nHo, Z.T. Jiang, L.Z. Zhang, Chem. Mater. 14 (2002) 3808–3816.
[19] W.T. Sun, Y. Yu, H.Y. Pan, X.F. Gao, Q. Chen, L.M. Peng, J. Am. Chem. Soc. 130 (2008) 1124–1125.
[20] R. Plass, S. Pelet, J. Krueger, M. Gratzel, U. Bach, J. Phys. Chem. B 106 (2002) 7578–7580.
[21] S.G. Hickey, D.J. Riley, E.J. Tull, J. Phys. Chem. B 104 (2000) 7623–7626.
[22] I. Robel, M. Kuno, P.V. Kamat, J. Am. Chem. Soc. 129 (2007) 4136–4137.
[23] I. Robel, V. Subramanian, M. Kuno, P.V. Kamat, J. Am. Chem. Soc. 128 (2006) 2385–2393.
[24] T. Ohmori, H. Takahashi, H. Mametsuka, E. Suzuki, Phys. Chem. Chem. Phys. 2 (2000) 3519–3522.
[25] K. Vinodgopal, P.V. Kamat, Environ. Sci. Technol. 29 (1995) 841–845.
[26] Z.H. Zhang, Y. Yuan, L.H. Liang, Y.X. Cheng, G.Y. Shi, L.T. Jin, J. Hazard. Mater. 158 (2008) 517–522.
[27] Z.H. Zhang, Y. Yuan, G.Y. Shi, Y.J. Fang, L.H. Liang, H.C. Ding, L.T. Jin, Environ. Sci. Technol. 41 (2007) 6259–6263.
[28] R. Enriquez, A.G. Agrios, P. Pichat, Catal. Today 120 (2007) 196–202.
[29] C.S. Turchi, D.F. Ollis, J. Catal. 122 (1990) 178–192.
[30] R.M. Gao, J. Stark, D.W. Bahnemann, J. Rabani, J. Photochem. Photobiol. A Chem. 148 (2002) 387–391.
[31] C.Y. Wang, C. Bottcher, D.W. Bahnemann, J.K. Dohrmann, J. Mater. Chem. 13 (2003) 2322–2329.
[32] K.S. Leschkies, R. Divakar, J. Basu, E. Enache-Pommer, J.E. Boercker, C.B. Carter, U.R. Kortshagen, D.J. Norris, E.S. Aydil, Nano Lett. 7 (2007) 1793–1798.
[33] A. Kongkanaed, K. Tvrdy, K. Takechi, M. Kuno, P.V. Kamat, J. Am. Chem. Soc. 130 (2008) 4007–4015.
[34] D.R. Baker, P.V. Kamat, Adv. Funct. Mater. 19 (2009) 805–811.
[35] Y. Hou, X.Y. Li, Q.D. Zhao, X. Quan, G.H. Chen, Adv. Funct. Mater. 20 (2010) 2165–2174.
[36] Z.B. Shao, W. Zhu, Z. Li, Q.H. Yang, G.Z. Wang, J. Phys. Chem. C 116 (2012) 2438–2442.
[37] S.K. Mohapatra, S. Banerjee, M. Misra, Nanotechnology 19 (2008) 315601.
[38] S. Shokhovets, O. Ambacher, G. Gobsch, Phys. Rev. B 76 (2007) 125203.
[39] X.N. Wang, H.J. Zhu, Y.M. Xu, H. Wang, Y. Tao, S.K. Hark, X.D. Xiao, Q. Li, ACS Nano 4 (2010) 3302–3308.
[40] C.G. Van de Walle, J. Neugebauer, Nature 5 (2003) 626–628.
[41] X.N. Wang, J. Wang, M.J. Zhou, H.J. Zhu, H. Wang, X.D. Cui, X.D. Xiao, Q. Li, J. Phys. Chem. C 113 (2009) 16951.